Characterisation of the apparent reflectance of a concrete calibration surface over different time scales

Karen Anderson[1] and Edward J. Milton[2]

[1] Department of Geography, University of Exeter, Tremough Campus, Penryn, Cornwall, TR10 9EZ, UK.
[2] School of Geography, University of Southampton, Highfield, Southampton, Hampshire, SO17 1BJ, UK.

ABSTRACT: This paper describes results from a detailed field spectral measurement campaign, designed to assess the temporal stability of calibration surface reflectance factors (ρ_λ). The results have wider implications for those using field measurements of reflectance in stand-alone studies, or in a calibration/validation context. A dual-field-of-view VNIR spectroradiometer system measured temporal changes in nadir ρ_λ at a concrete calibration surface. Reflectance factor variations were assessed in relation to the solar zenith angle (SZA), using the modified Walthall *et al.* (1985) model. Superimposed on low-magnitude variations in ρ_λ with SZA, were larger differences caused by environmental effects. Seasonal changes were caused by activation of a vegetative bloom which caused ρ_λ to vary by up to 16% (670nm). A smaller amount of variation was associated with changes in total solar radiation (kWm^{-2}). This was an 'apparent' effect, caused by the directional anisotropy of the surface response, in relation to changing distributions of irradiance. A quantitative surface response model was derived empirically, and successfully used to predict concrete ρ_λ. The results highlight fundamental differences between inherent and apparent reflectance, and demonstrate that the reflectance factor response of a weathered concrete calibration surface was predictable over a range of timescales.

INTRODUCTION

Remote sensing provides the means to make scientific measurements of the Earth on a global scale, but to ensure that such data have lasting quantitative value, they must be calibrated to meaningful physical units and the uncertainty associated with them must be quantified (Fox 2001). In the optical domain, spectral reflectance is a variable of primary importance; not only is it important in its own right, but other key variables can also be derived from it (e.g. albedo).

Reflectance data collected in the natural environment are only ever approximations of 'inherent' surface properties. The inherent reflectance response is defined by the bidirectional reflectance distribution function (BRDF), and includes the spatial and geometric arrangement of surface elements (Barnsley *et al.* 1994), and their wavelength-dependent optical properties (Gao e*t al.* 2003). In contrast, hemispherical-directional reflectance factors (HDRF) measured under solar illumination are an 'apparent' quantity, because the measured signal may vary in relation to angles of illumination and view, and according to differing distributions of hemispherical irradiance (Kriebel 1976, Milton 1981). Methods exist to *infer* inherent reflectance properties from measurements of apparent reflectance, for instance by modelling changes in apparent ρ_λ in response to solar zenith angle variations (Walthall *et al.* 1985).

The aim of this experiment was to create a numerical model to describe variations in the spectral reflectance of a ground calibration target (GCT) over different time scales. GCTs perform several important functions in quantitative remote sensing. They are used for vicarious calibration of satellite sensors (Thome *et al.* 1998), for atmospheric correction (Moran *et al.* 2001), and for validating radiative transfer models (Jacob *et al.* 2004). The spatial uniformity of GCTs is often studied in great detail, but much less attention is directed to their temporal stability. Furthermore, their inherent reflectance is often assumed to be constant, especially if they are constructed of materials such as concrete or asphalt.

TEST SITE

The test site was a disused military airfield on Thorney Island (50°48'27"N, 0°55'32"W), West Sussex, UK (Figure 1). The UK has several hundred similar airfields, many of which are relics from World War II. Many such sites still have large concrete and asphalt areas intact, which would be suitable GCTs for use with fine spatial resolution sensors. The focus of this experiment was an instrumented concrete GCT at the southern end of the main north-south runway (Anderson 2005).

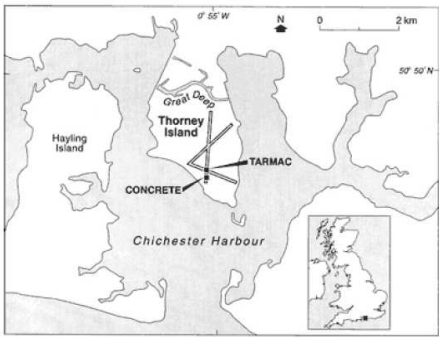

Figure 1: Location map of Thorney Island, West Sussex, UK.

METHODOLOGY

The research employed a dual-field-of-view (DFOV) GER1500 spectroradiometer system in which two sensor heads were used to collect HDRFs in the range 400-1000nm. The cos-conical system enabled reference (downwelling irradiance) and target (upwelling radiance) measurements to be made simultaneously, producing more precise field spectra than a traditional 'single-beam' approach (Duggin 1980, Rollin *et al.* 1998). The two sensor heads were inter-calibrated in the field on each visit (Anderson and Milton (in press)). Reflectance factors were calculated according to Equation 1, where $CCcal_\lambda$ is the inter-calibration function, E_λ is the reference sensor signal, and LT_λ is the target sensor signal.

$$\rho_\lambda = \left(\frac{LT_\lambda}{E_\lambda} \right) \times CCcal_\lambda \qquad (1)$$

High spatial positioning precision was ensured through use of a specially designed mobile spectroradiometer. The repeatability of reflectance measurements made with this device was estimated as ±0.95% at 700 nm (Anderson 2005).

RESULTS

A. *Short-term variations in ρ_λ with solar zenith angle*

The first part of the analysis aimed to determine the anisotropy of the concrete response to varying angles of illumination. It was therefore necessary to use a finite measurement sequence, so as to limit the analysis to a period where the main variable was solar zenith angle (SZA). Concrete reflectance factors collected over a one-hour period on 14th July 2003 were used for this part of the study (Table 1). The average proportion of diffuse to global flux over this period was 0.164 (at 550 nm), indicating that 16.4% of the total irradiance was from skylight. This demonstrates that atmospheric conditions were favourable for optical remote sensing during this time period.

TABLE 1. MEASUREMENT CONDITIONS ON 14TH JULY 2003.

Surface	Start time (GMT)	End time (GMT)	No. of scans	Mean DG ratio	Median SZA	Range SZA
Concrete	10:08	11:02	144	0.164	34.57°	5.4°

The modified Walthall *et al.* (1985) model was used for quantifying reflectance factor responses to SZA, because it made no assumption about the nature of the target (Barnsley *et al.* 1994). In this model, the relationship between ρ_λ and SZA simplifies to Equation 2, when measurements at nadir are used (i.e. θ_r=0°), assuming no azimuthal structure at the surface. This results in a squared relationship between ρ_λ and SZA (θ_i), where a_λ and b_λ can be empirically derived.

$$\rho_\lambda = (a_\lambda \theta_i^2) + b_\lambda \qquad (2)$$

Results demonstrated that concrete reflectance factors could be described in relation to changes in θ_i^2, according to Equation 2. Figure 2 shows the concrete ρ_λ response to SZA variations. Those data points significantly above the dashed line show reflectance measurements which deviated from the response predicted by the Walthall model. The fact that the majority of the data points conform to the model suggests that an episodic or intermittent factor caused the overestimated values, rather then a systematic failure of the model or a bias in the instrument used. Enlargement of the region around SZA=32.5° shows that some of this variability might relate to variations in the DG ratio (Figure 3). A plausible physical mechanism for this would be the enhanced apparent reflectance of the concrete surface as the proportion of diffuse irradiance increased.

Linear regression results of ρ_λ on θ_i^2 (excluding 13 spurious points) are given in Table 2, where results from six channels summarise the main trends. All slope coefficients were negative (Table 2), caused by increased shadowing contributions from aggregate particles as SZA increased. Mean Absolute Differences (MAD_λ) between measured ($m_{\rho\lambda}$) and modelled ($M_{\rho\lambda}$) reflectance factors were calculated according to Equation 3, to enable cross-comparison with results published by Moran *et al.* (2001). Low-magnitude scatter around the model line (excluding previously discussed data points) arose from slight variations in atmospheric state, and measurement uncertainty, which was quantified as contributing ±0.0023% of the signal at 700nm.

$$MAD_\lambda = \frac{1}{n}\sum_{i=1}^{n}\left|M\rho_{\lambda,i} - m\rho_{\lambda,i}\right| \qquad (3)$$

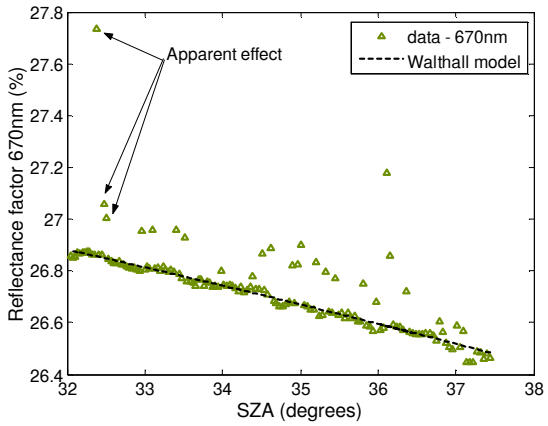

Figure 2: Variation in concrete reflectance factors at 670nm, in relation to SZA (14th July 2003). The Walthall model is shown as a dashed line.

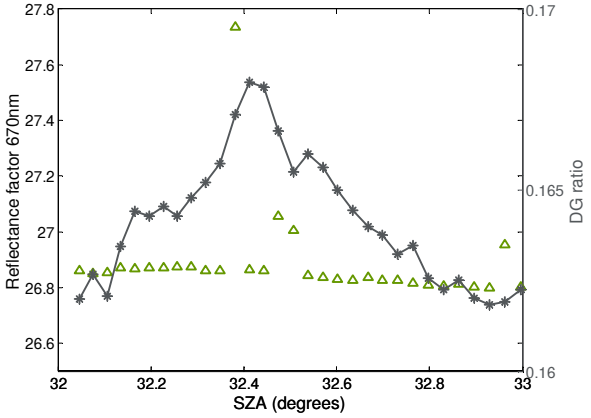

Figure 3: The effect of changing distributions of irradiance on reflectance factor responses to SZA (DG ratio = grey line; concrete reflectance factor = triangle).

TABLE 2. APPLICATION OF THE WALTHALL MODEL TO FIELD-MEASURED REFLECTANCE FACTORS OF TWO SURFACES

λ (nm)	a_λ	b_λ	R^2	MAD_λ (% refl)
490	-4.44×10^{-4}	19.68	0.845	0.0128
552	-1.54×10^{-3}	25.79	0.890	0.0489
670	-1.05×10^{-3}	27.96	0.952	0.0148
750	-9.79×10^{-4}	29.73	0.922	0.0191
780	-1.00×10^{-3}	30.38	0.921	0.0202
865	-9.67×10^{-4}	32.44	0.870	0.0284

B. Seasonal variations in ρ_λ

Seasonal trends in reflectance factors measured on 25 separate occasions over the 2002-2004 period were subsequently analysed. Underlying signal variations caused by daily changes in SZA were apparent in each of the measurement sequences, where low magnitude negative trends with increasing SZA were present; but y-intercept values for each of these linear relationships were not consistent through time (Figure 4). Additionally, seasonal variations in ρ_λ were much larger than could be explained by SZA alone. For example, at 670nm, reflectance factors measured on 25 dates over a three-year period varied by up to 16% reflectance (Figure 4). This variation greatly exceeded the maximum spectral variation introduced by positional uncertainty in the mobile device. Seasonality was also present. Reflectance factors measured in mid-April were low in all wavelength channels, while those measured in late-summer and autumn were typically higher. As a result there was a notable seasonal brightening of the surface throughout the year (Figure 4). Subsequent investigations aimed to resolve the physical mechanisms underpinning these seasonal variations through use of an empirical model.

The first part of the analysis removed underlying signal variations caused by seasonally variable SZA. This utilised the 'clear sky' response model previously described (Figure 4 overlays this on seasonal data). Residuals from this model were then assessed in relation to other environmental variables.

Lower values of ρ_λ in April, coupled with the presence of a more pronounced darkening in visible wavelengths (and less so in NIR) at this time of year, provided an initial indicator that the calibration surface was subject to a seasonally-variable vegetative bloom. The clearest patterning in residuals was found when residuals were plotted against a normalised vegetation index calculated using the 665nm (red) and 990nm (NIR) channels (Equation 4). Figure 5 shows the mean residuals from each measurement sequence, and suggests a negative relationship with NDVI, indicating that NDVI was acting as an index of the darkening of the surface. Similar trends were found throughout the VNIR spectrum.

$$NDVI = \frac{\rho_{990nm} - \rho_{665nm}}{\rho_{990nm} + \rho_{665nm}} \qquad (4)$$

Results showed that NDVI accounted for between 61.9% (865nm) and 87.6% (490nm) of the residuals from 'clear sky' behaviour. There was evidence of wavelength-dependency in these results with the best fit being achieved at 490nm and a progressive decline in the ability of the model to explain deviations at longer wavelengths. This may have been caused by lower signal-to-noise ratios at longer wavelengths, or a lower dependence on vegetation amount in longer wavelengths. Residuals were both positive and negative in magnitude (Figure 5), because they were referenced to a mid-summer dataset collected on 14th July 2003, when the vegetative bloom had started to die back due to water limitation and desiccation.

Further analysis aimed to determine whether any remaining variability in ρ_λ could be described using other environmental variables. Residuals from a linear model incorporating both θ_i^2 and NDVI were analysed. Total solar radiation (TSR; kWm^{-2}) measured by a broadband pyranometer explained a small amount of residual variability in ρ_λ, and was a surrogate for the irradiance anisotropy and its effect on apparent reflectance. Inclusion of a DG ratio term was inconclusive.

C. Development of a quantitative model for concrete

Extensive investigations into the effects of each of the three variables (θ_i^2, NDVI and TSR) on ρ_λ, highlighted that these were best combined into a linear model described by Equation 5. Empirically-derived coefficients are provided in Table 3.

$$\hat{\rho}_\lambda = (a_\lambda \theta_i^{\,2}) + (b_\lambda NDVI) + (c_\lambda TSR) + d_\lambda \qquad (5)$$

The model can be visualised in Figure 6, where the y-intercept value (ρ_λ) of the Walthall-predicted behaviour to SZA (i.e. Figure 3) was modified by NDVI and/or TSR. For a given TSR (in Figure 6, TSR = 0.35 kWm^{-2}), the y-intercept value of the squared relationship between ρ_λ and θ_i varies according to NDVI. Similar patterns were seen when TSR varied (constant NDVI); although the effect of TSR was much smaller.

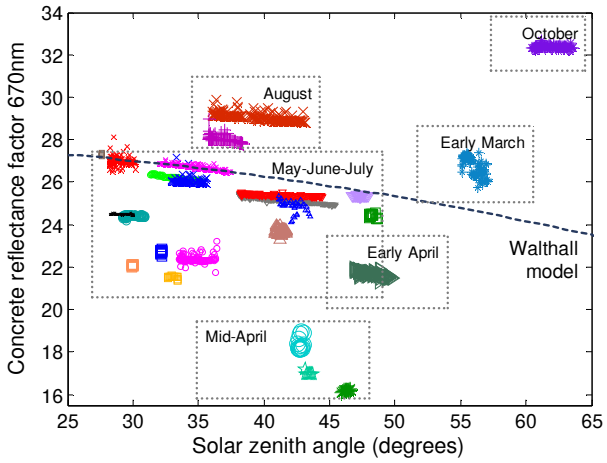

Figure 4: Temporal variation in reflectance factors of the concrete surface on 25 occasions during the 2002-2004 measurement period, at 670nm. The Walthall model derived using 14th July 2003 data is overlaid.

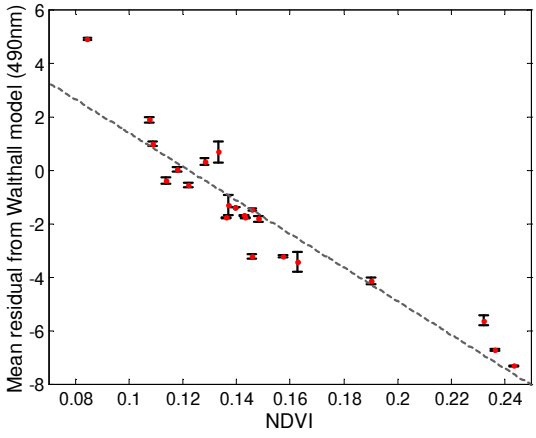

Figure 5: Mean residuals from the Walthall model at 490nm (+/-1SD), plotted against NDVI.

TABLE 3. MODEL COEFFICIENTS DESCRIBING CONCRETE REFLECTANCE FACTOR RESPONSES OVER THE 2002-2004 FIELD SEASON (TRAINING DATASET COMPRISING 1340 SAMPLES)

λ nm	a_λ	b_λ	c_λ	d_λ	R^2	*RMSE*
490	-4.44×10^{-4}	-77.12	-3.575	31.70	0.931	0.577
552	-1.54×10^{-3}	-92.71	-7.839	43.19	0.826	1.241
670	-1.05×10^{-3}	-97.08	-6.029	44.79	0.848	1.164
750	-9.79×10^{-4}	-89.44	-6.732	46.35	0.812	1.242
780	-1.00×10^{-3}	-86.09	-6.870	46.74	0.791	1.289
865	-9.67×10^{-4}	-74.28	-6.647	47.22	0.760	1.237

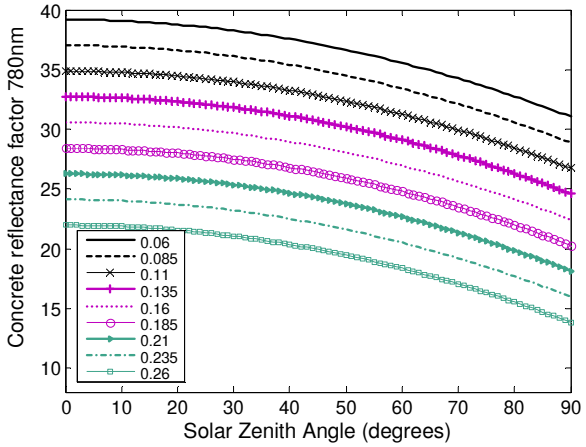

Figure 6: Results of the concrete model run on a range of hypothetical NDVI values at 780nm. TSR was fixed at 0.35 kWm^{-2}. NDVI values are indicated in the legend text.

D. Model testing

The model was tested on two independent datasets, the first was a subset of the original data, not included in model development (every other data point was used to derive the model (n=1340, table 3) and the remaining 1340 data points were used as a test dataset). Here, RMSEs between modelled and measured ρ_λ ranged between 0.588 (490nm) and 1.306 (780nm). The second test dataset comprised sequences of measurements collected at the concrete calibration site on three dates during a pilot study. Here, the model was found to produce RMSEs of less than 1.2% in all wavelengths (as low as 0.43% in visible channels) with summer and autumn datasets. With test data collected in spring, RMSEs were higher (<2%). In contrast to the summer dataset, spring-modelled ρ_λ deviated from measured ρ_λ to the greatest extent in visible wavelengths. This was attributed to the limited spectral characterisation of the full variation in the spring algal bloom, which exerted the largest effect on visible ρ_λ.

SUMMARY

This study has demonstrated that weathered concrete calibration surfaces, measured in a mid-latitude temperate environment do not maintain stable reflectance factor responses over a range of timescales.

Variations in ρ_λ over short timescales, measured in optimal atmospheric conditions were quantified using the Walthall *et al.* (1985) model where SZA was the descriptor variable. Complex variations in concrete ρ_λ over seasonal timescales were also demonstrated in relation to both inherent and apparent effects. SZA explained low-magnitude variations in seasonal data, but an algal bloom was responsible for most of the remaining variation in ρ_λ - an inherent surface change detected by an apparent indicator (NDVI). Some additional variability in ρ_λ was described by inclusion of a TSR term, supporting the notion that dual-beam measurements may 'fail to compensate for all the consequences of atmospheric changes', due to differing anisotropies of the reference and target scenarios in the field environment (Milton, 1981).

REFERENCES

[1] Anderson, K. (2005). Temporal variability in calibration surface reflectance: methods models and applications. *PhD thesis*, University of Southampton, 381pp.

[2] Anderson, K. and Milton, E. (in press). Calibration of dual-beam spectroradiometric data, *International Journal of Remote Sensing*.

[3] Barnsley, M., Strahler, A., Morris, K. and Muller, J.-P. (1994). Sampling the surface bidirectional reflectance distribution function (BRDF): 1. Evaluation of current and future satellite sensors, *Remote Sensing Reviews* 8: 271–311.

[4] Duggin, M. (1980). The field measurement of reflectance factors, *Photogrammetric Engineering and Remote Sensing* 46: 643–647.

[5] Fox, N. (2001). Traceability to SI for EO measurements. *CEOS WGCV Cal/Val Newsletter 9*, January 2001, 1-9.

[6] Gao, F., Schaaf, C. B., Strahler, A. H., Jin, Y. and Li, X. (2003). Detecting vegetation structure using a kernel-based BRDF model, *Remote Sensing of Environment* 86(2): 198–205.

[7] Jacob, F., Petitcolin, F., Schmugge, T., Vermote, E., French, A., and Ogawa, K. (2004). Comparison of land surface emissivity and radiometric temperature derived from MODIS and ASTER sensors, *Remote Sensing of Environment*, 90: 137-142.

[8] Kriebel, K. (1976). On the variability of the reflected radiation due to differing distributions of irradiance, *Remote Sensing of Environment* 4: 257–264.

[9] Milton, E. (1981). Does the use of two radiometers correct for irradiance changes during measurements?, *Photogrammetric Engineering and Remote Sensing* 47(8): 1223–1225.

[10] Moran, M., Bryant, R., Thome, K., Ni, W., Nouvellon, Y., Gonzalez-Dugo, M., Qi, J. and Clarke, T. (2001). A refined empirical line approach for reflectance factor retrieval from Landsat-5 TM and Landsat-7 ETM+, *Remote Sensing of Environment* 78: 71–82.

[11] Rollin, E., Emery, D., Kerr, C. and Milton, E. (1998). Dual-beam reflectance measurements and the need for a field inter-calibration procedure, in P. Burt, C. Power and P. Zukowskyj (eds), *Developing International Connections: Proceedings of the 24th Annual Conference of the Remote Sensing Society*, Nottingham, UK, pp. 552–558.

[12] Thome, K., Schiller, S., Conel, J., Arai, K. and Tsuchida, S. (1998). Results of the 1996 Earth Observing System vicarious calibration joint campaign at Lunar Lake Playa, Nevada (USA), Metrologia 35: 631–638.

[13] Walthall, C., Norman, J.,Welles, J., Campbell, G. and Blad, B. (1985). Simple equation to approximate the bidirectional reflectance from vegetative canopies and bare surfaces, *Applied Optics* 24(3): 383–387.

Karen Anderson, email address (karen.anderson@exeter.ac.uk)

Edward J. Milton, email address (E.J.Milton@soton.ac.uk)